

# Preparation of CuO Thin Films by Thermally Oxidized Metallic Cu Films for CdS/CuO Heterojunction Diode

Ngamnit Wongcharoen\* and Thitinai Gaewdang

*Department of Physics, Faculty of Science, King Mongkut's Institute of Technology Ladkrabang, Bangkok 10520, Thailand*

*\*Corresponding author. E-mail: ngamnit.wo@kmitl.ac.th*

## ABSTRACT

*Copper thin films were deposited on glass substrates using thermal evaporation in vacuum and then thermally oxidized in air at temperatures of 100-500°C. XRD patterns showed the formation of a fine grain Cu<sub>2</sub>O phase at 300°C and a CuO phase at 400°C, respectively. Crystallinity and grain size improved with increasing oxidation temperature. The energy gap of the samples evaluated from absorption measurements was 2.10-2.23 eV. Important electrical parameters of the CuO thin films obtained from oxidizing at 500°C were resistivity of  $8.53 \times 10^3 \Omega \cdot \text{cm}$ , carrier concentration of  $7.60 \times 10^{13} \text{ cm}^{-3}$ , and mobility of  $6.22 \text{ cm}^2/\text{V}\cdot\text{s}$ . A prototype of a CdS/CuO thin-film heterojunction diode was successfully prepared by thermal evaporation of CdS thin films on CuO thin-film substrate in a vacuum. The obtained device exhibited a good rectifying behavior from I-V characteristics. Junction parameters calculated using I-V data were barrier height of 5.190 eV, ideality factor of 0.520, and series resistance of  $3.87 \Omega$ . Impedance spectroscopy of the device was investigated at temperatures of 25-60°C. The real and imaginary parts of the complex impedance changed with the temperature and frequency. The experimental results suggested that the device was a good candidate for photovoltaic devices with low thermal budget and low product cost.*

**Keywords:** CuO thin films, Thermal oxidation, CdS/CuO heterojunction, Impedance spectroscopy

## INTRODUCTION

Copper oxides are semiconducting materials that have a natural abundance of starting material Cu. They have been extensively studied because of their potential applications in solar cells, gas sensors, electrochemical sensors, and batteries (Valladares, 2012; Ooi et al., 2013). Copper oxides are composed of two oxide phases, namely, cupric oxide (CuO) and cuprous oxide (Cu<sub>2</sub>O) with p-type conductivity; the former has a narrow band gap of 1.21-1.51 eV absorbing throughout the visible spectrum with a monoclinic structure, while the latter has a direct optical band gap of 2.10-2.60 eV with a cubic structure (Cho et al., 2013). A meta-stable copper oxide, Cu<sub>4</sub>O<sub>3</sub>, which is an intermediate compound between

the previous two, has also been reported (Ooi et al., 2013). Numerous methods such as reactive sputtering, chemical vapor deposition, sol-gel, electro-deposition, and thermal oxidation have been used to grow copper oxide thin films. In this work, we investigated the effect of temperature of oxidation on the properties of copper oxide thin films prepared by oxidation of thermal vacuum evaporated Cu thin films. We studied the structural, optical, and electrical properties of the films to assess their potential use in p-n junctions. The formation of CdS/CuO heterojunction was elaborated by thermal evaporation of CdS thin films on CuO thin films coated on an ITO glass substrate. We investigated I-V and C-V characteristics of the CdS/CuO heterojunction to evaluate some important parameters, including junction barrier height, ideality factor, and series resistance values, by using thermionic emission theory and Cheung's method. Moreover, impedance spectroscopy of the device was investigated at a temperature range of 25-60°C.

## MATERIALS AND METHODS

### Preparation and characterization of thin films for CdS/CuO diode

Copper thin films were grown on glass substrates by thermal evaporation in a vacuum better than  $5 \times 10^{-5}$  mbar. Before deposition, the glass substrates were cleaned in acetone, ethanol, and de-ionized water, in succession. The starting material was metallic Cu pellets (99.99% purity). The film thickness of about 200 nm was monitored by a quartz crystal thickness monitor (Edward type FTM 6). The thermal oxidation of Cu films was carried out in a muffle furnace at different temperatures, ranging from 100-500°C, for 60 min. The heating rate was maintained at 100°C/h. After soaking at the desired temperature for 60 min, the furnace was turned off, allowing the samples to cool to room temperature naturally. The crystal structure of these films was checked by X-ray diffraction technique with a Bruker D 8 diffractometer using  $\text{CuK}\alpha$  radiation. Surface morphology was examined by a scanning electron microscope (JEOL model JSM-6400). A UV-VIS double beam spectrophotometer measured optical absorption in the wavelength range of 220-800 nm. The band gap ( $E_g$ ) of the transparent films was determined by the equation  $(\alpha hv)^2 = A'(hv - E_g)$ , where  $\alpha$  is the absorption coefficient,  $A'$  is a constant, and  $hv$  is the photon energy. The absorption coefficient ( $\alpha$ ) was calculated by using the relation  $\alpha = 2.303A/d$ , where  $A$  is the absorbance and  $d$  is the thickness of the sample. The  $(\alpha hv)^2$  data were obtained from optical absorbance measurements and, following the method reported by Tauc, were plotted as a function of photon energy ( $hv$ ) to estimate the energy gap ( $E_g$ ).

Electrical properties of the films were evaluated by Hall effect and resistivity measurements in the van der Pauw configuration at room temperature. To fabricate the CdS/CuO thin film heterojunction, Cu thin films were deposited on ITO-coated glass substrate and oxidized at 500°C for 60 min. CdS thin films were subsequently evaporated onto CuO films. Finally, an ohmic contact was made with silver paste on the surface of CdS and on the surface of ITO.

**Electrical transport model**

Based on the thermionic emission (TE) mechanism, current flows in a semiconductor diode is given by the relations (Rhoderick and William, 1988):

$$I = I_S \exp\left(\frac{qV}{nkT}\right) [1 - \exp(-qV/kT)] \tag{1}$$

and 
$$I_S = AA^*T^2 \exp\left(-\frac{q\phi_{B0}}{kT}\right) \tag{2}$$

where  $I_S$  is the saturation current derived from the straight line intercept of the semi-logarithmic I-V plot at  $V=0$ ;  $V$  is forward bias voltage;  $T$  is the absolute temperature;  $q$  is the electronic charge;  $k$  is the Boltzmann constant;  $A$  is the effective area;  $A^* = 4\pi qm_e/h^3$  is the effective Richardson constant of  $20 \text{ A}\cdot\text{cm}^{-2}\cdot\text{K}^{-2}$  for n-CdS, where  $m^*=0.165m_0$  is the effective mass of the electrons;  $\phi_{B0}$  is the apparent barrier height at zero bias voltage; and  $n$  is the ideality factor. Once  $I_S$  is known from a least square fit of equation (1) to the linear part of the measured semi-logarithmic I-V plot, the zero bias barrier height ( $\phi_{B0}$ ) can also be computed with the help of equation (2). From equation (1), the ideality factor  $n$  is given by:

$$n = \frac{q}{kT} \frac{dV}{d(\ln I)} \tag{3}$$

Cheung proposed an efficient technique to determine  $RS$ ,  $n$ , and  $\phi_{B0}$  (Aksoy and Cagar, 2014). From equation (1), the following functions can be written as:

$$\frac{dV}{d(\ln I)} = \frac{nkT}{q} + IR_S \tag{4}$$

$$H(I) = V \left( n \frac{kT}{q} \right) \ln \left( \frac{I}{AA^*T^2} \right) \tag{5}$$

and  $H(I)$  is given as:

$$H(I) = n\phi_B + IR_S \tag{6}$$

where  $\phi_{B0}$  is the barrier height obtained from data of downward curvature region in the forward bias I-V characteristics.

**Electrical characterization of diode**

The I-V characteristic curves were measured by a computer-interfaced Keithley 236 current/voltage source at room temperature. The bias voltage used was from -0.5 to 1.0 V. Impedance spectroscopy was carried out by Agilent E4980A Precision LCR Meter with frequency range of 10 kHz - 2 MHz and temperature range of 25-60°C.

## RESULTS

### Cu-O films characteristics

The XRD patterns of the as-grown and thermally oxidized Cu films at different temperatures ranging from 100-500°C are shown in Figure 1. The as-grown Cu sample revealed a diffraction peak at  $2\theta$  equal to  $43.50^\circ$  that corresponded to the (111) diffraction plane of metallic Cu. Oxidation of Cu thin films at 100 and 200°C still showed the purely (111) diffraction plane of metallic Cu phase, with reduction in peak intensity. For the sample Cu films oxidized at 300°C, a weak diffraction peak at  $36.46^\circ$  corresponding to the (111) plane of  $\text{Cu}_2\text{O}$  was observed. However, at an oxidation temperature of 400°C, the (-111) diffraction plane of monoclinic CuO phase occurred. For the films oxidized at 500°C, two well-resolved diffraction peaks at  $2\theta$  of  $35.40^\circ$  and  $38.35^\circ$  were observed. These peaks correspond to diffraction of the (-111) and (111) planes of standard JCPDS data of CuO (JCPDS No. 80-1268). Figure 2 shows the SEM micrograph of Cu films oxidized at 100, 300, and 500°C. The surface of the as-deposited Cu films was mostly smooth and uniform, while the surface particle size and surface roughness increased with increasing thermal oxidation temperature.

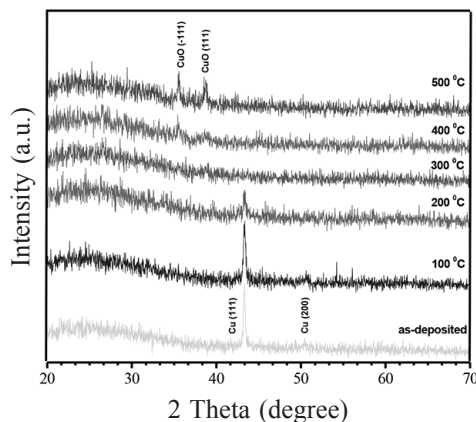


**Figure 1.** XRD patterns of CuO films.

Electrical properties of the films were evaluated by Hall effect and resistivity measurements in the van der Pauw configuration. Cu films oxidized at 100-500°C exhibited p-type conductivity. Variations of the resistivity ( $\rho$ ), carrier concentration ( $p$ ), and mobility ( $\mu$ ) against oxidation temperature are shown in Figure 3. The as-deposited and the Cu films oxidized at 100°C showed very low resistivity ( $\sim 10^{-4} \Omega\cdot\text{cm}$ ). In contrast, the films oxidized at temperatures beyond 200°C showed high resistivity, on the order of  $10^3 \Omega\cdot\text{cm}$ . The carrier concentration initially decreased as the oxidation temperature increased up to 300°C, and then increased at higher oxidation temperatures. The mobility gradually decreased from 31.28 to 6.22  $\text{cm}^2/\text{V}\cdot\text{s}$  as the oxidation temperature increased from 100 to 500°C.

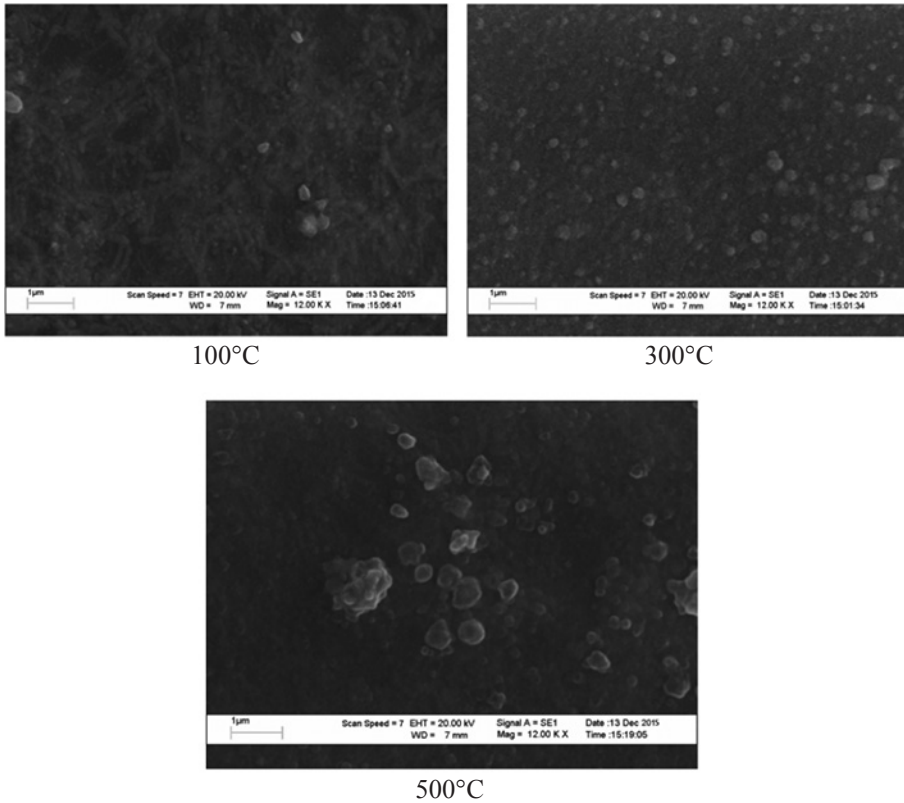


**Figure 2.** SEM micrographs of CuO films oxidized at 100, 300, and 500°C.

Figure 4 shows the absorbance ( $A$ ) as a function of wavelength for the films oxidized at different temperatures. The absorbance value decreased as the wavelength increased. Figure 5 displays the plot of the energy gap of the films oxidized at 300°C calculated using Tauc's method. Variation of energy gap as a function of oxidation temperature is shown in Figure 6. The  $E_g$  value initially increased up to the maximum value 2.23 eV at an oxidation temperature of 300°C, and then decreased to the minimum value 2.10 eV at 500°C.

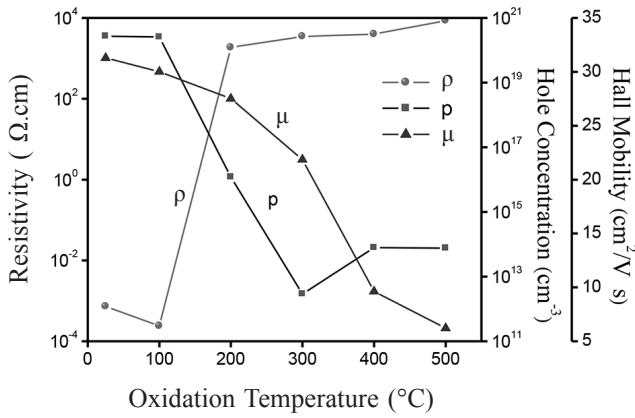


Figure 3. Variation of  $\rho$ ,  $p$ , and  $\mu$  of CuO films.

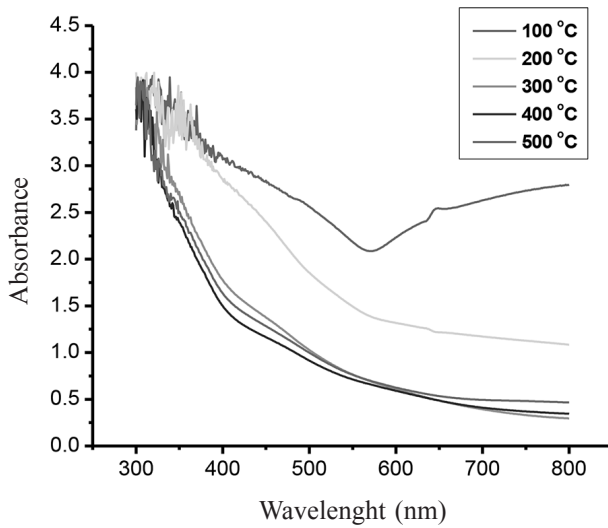
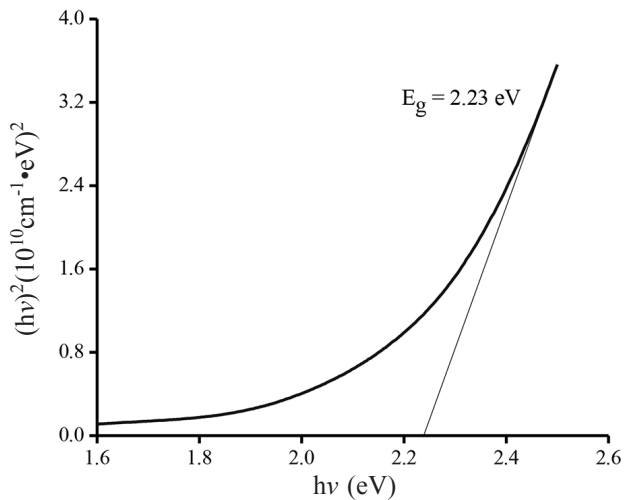
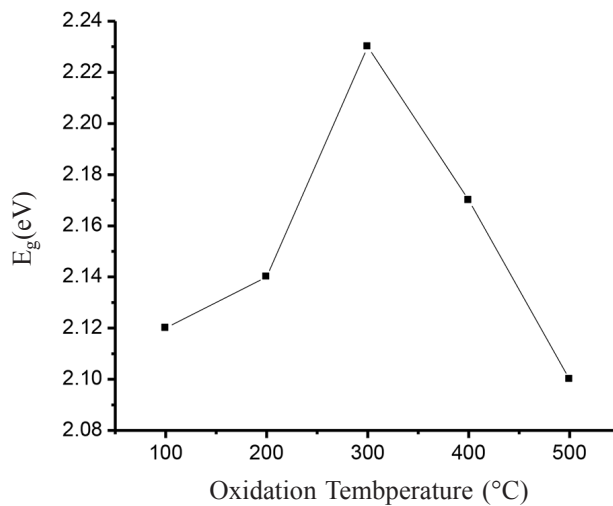


Figure 4. Absorption spectra of CuO films.



**Figure 5.** Plot of  $(h\nu)^2$  vs.  $h\nu$  of CuO films oxidized at 300°C.



**Figure 6.** Variation of  $E_g$  with oxidation temperature.

### Device characteristics

The measured I-V plot of CdS/CuO diode at room temperature is shown in Figure 7. Figure 8 shows the semi-logarithmic I-V plot within bias voltage of about 0.1-0.4 V. From Equations (2) and (3), the experimental value of the ideality factor and barrier height were 5.190 and 0.520 eV, respectively. The  $\ln I$ - $\ln V$  plot is presented in Figure 9. According to Cheung's model, the plots of  $dV/d(\ln I)$  vs.  $I$  and  $H(I)$  vs.  $I$  are shown in Figures 10 and 11, respectively.

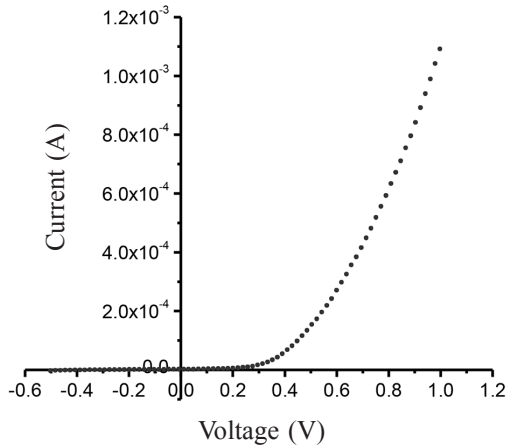


**Figure 7.** I-V plot of CdS/CuO diode.

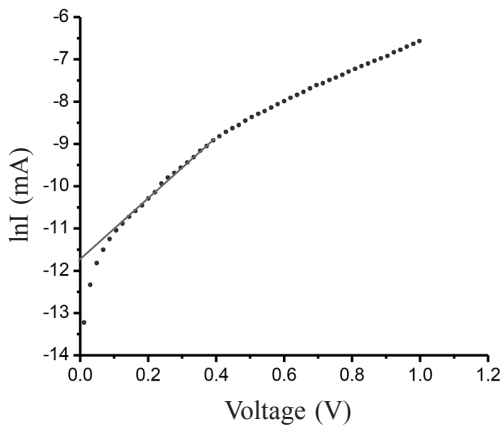


**Figure 8.**  $\ln I$ -V plot of CdS/CuO diode.



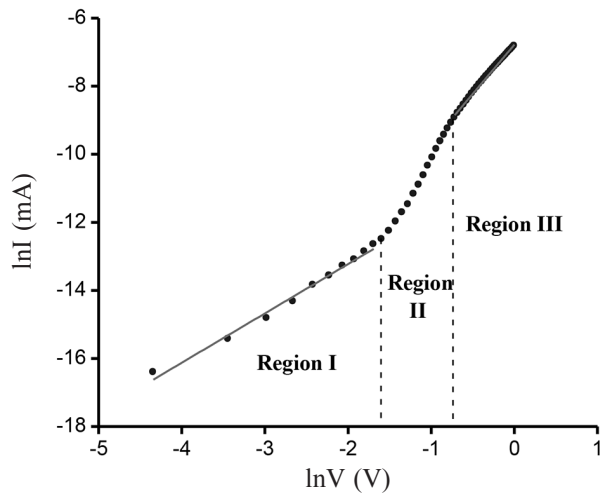


Figure 9.  $\ln I$ - $\ln V$  plot of CdS/CuO diode.

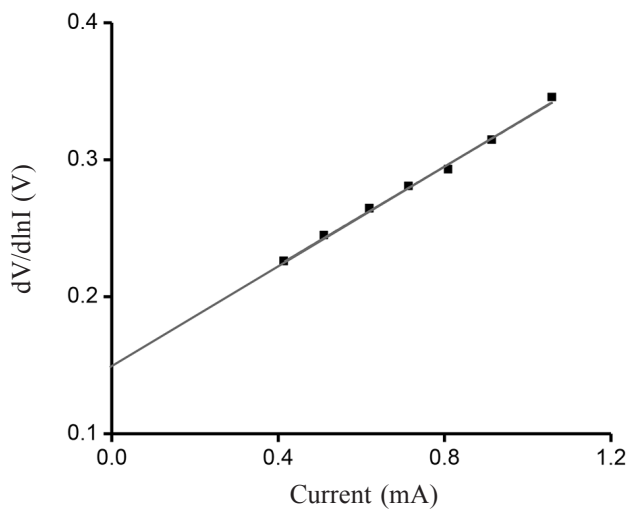
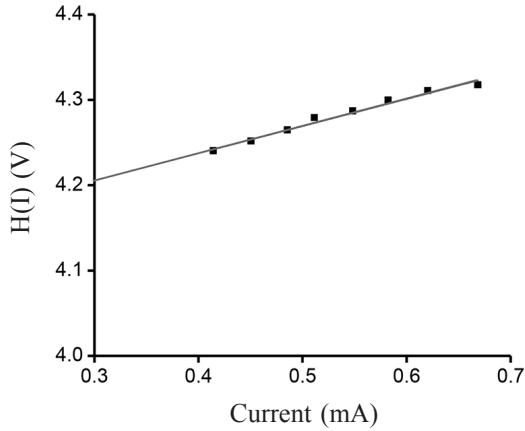
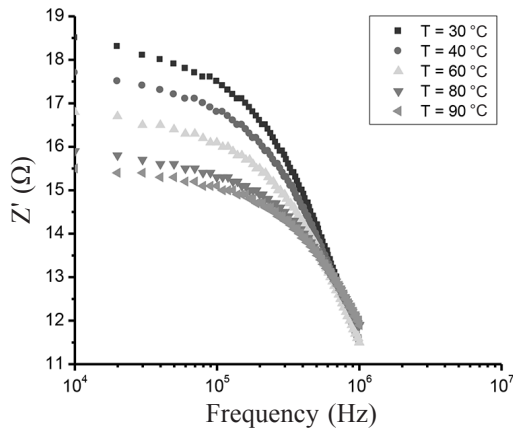


Figure 10.  $dV/d(\ln I)$ -I plot of CdS/CuO diode.



**Figure 11.** H(I)-I plot of CdS/CuO diode.

The variations in the real ( $Z'$ ) and imaginary ( $Z''$ ) parts of complex impedance with frequency at different temperatures are shown in Figures 12 and 13, respectively. The relaxation frequency ( $\omega_0$ ) was obtained from the peak frequency of  $Z''$ -f plot. The Arrhenius plot of  $\ln(\omega_0/T^2)$  is shown in Figure 14.



**Figure 12.**  $Z'$ -f plot of CdS/CuO diode.

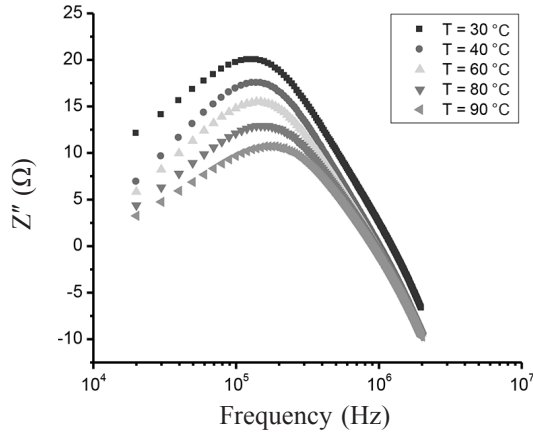


**Figure 13.** Z'-f plot of CdS/CuO diode.

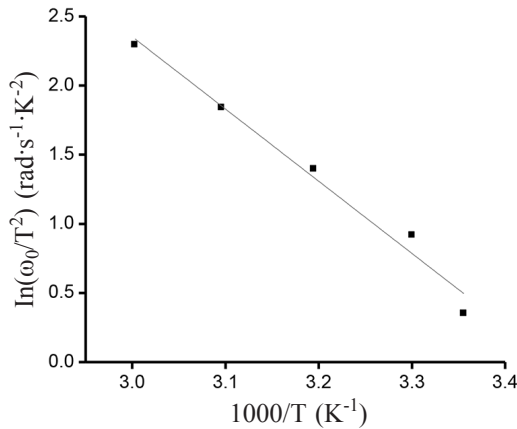


**Figure 14.** Arrhenius plot of  $\ln(\omega_0/T^2)$ .

### DISCUSSION

The as-grown CdS/CuO heterojunction showed a good rectifying behavior. The observed high ideality factor ( $>1$ ) of the diode suggested that the thermionic emission model did not define well the device’s transport properties. To better understand the mechanism that controls the transport properties of this heterojunction, a  $\ln I$ - $\ln V$  plot was presented. It is evident from the  $\ln I$ - $\ln V$  plot that forward bias characteristics showed three regions. The I-V characteristics of region I ( $V < 0.1\text{V}$ ) complied with linear ohmic behavior ( $I \sim V$ ), which is mainly caused by thermally generated charge carriers (Tyaki et al., 2015). In region II ( $0.1 \leq V \leq 0.4\text{V}$ ), the current increased exponentially with bias voltage ( $I \sim \exp \alpha V$ ). This is mainly due to the recombination-tunneling mechanism (Aksoy and Cagar, 2012). At higher bias voltage (region III,  $V > 0.4\text{V}$ ), the I-V characteristics

followed a power law relation ( $I \sim V^2$ ). The current flow through the junction is due to space-charge limited current (SCLC) conduction, dominated by a single energy trap level (Zeyada et al., 2015). This SCLC mechanism is a normal phenomenon in a wide band gap semiconductor (Tyaki, 2015).

The series resistance ( $R_s$ ) is an important parameter in the electrical characteristics of a diode. This parameter is significant in the downward curvature (non-linear region) of the forward bias I-V characteristics; but the other two parameters ( $n$  and  $\phi_{B0}$ ) are significant in both the linear and non-linear regions of the I-V characteristics. Equation (4) should give a straight line for the data of the downward curvature region in the forward bias I-V characteristics. Thus, a plot of  $dV/d(\ln I)$ -I will give  $R_s$  as the slope and  $nkT/q$  as the y-axis intercept. The values of  $n$  and  $R_s$  were calculated as 5.322 and 3.48  $\Omega$ , respectively. This  $n$  value is slightly different from that obtained from the forward bias  $\ln I$ -V plot. This difference may be caused by the presence of series resistance and interface states (Aksoy and Cagar, 2012). Using the  $n$  value determined from equation (4) and the data of the downward curvature region in the forward bias I-V characteristics in equation (5), a plot of  $H(I)$ -I should generate a straight line with the y-axis intercept equal to  $n\phi_{B0}$ . The slope of this plot also determines  $R_s$ , which can be used to check the consistency of this approach. From Figure 11, the barrier height and series resistance of the device were calculated as 0.542 and 3.87  $\Omega$ , respectively. Furthermore, the values of  $R_s$  obtained from the  $dV/d(\ln I)$ -I and  $H(I)$ -I plots were in good agreement with each other, indicating the consistency of Cheung's approach.

Figure 12 represents the variation of the real part ( $Z'$ ) of complex impedance as a function of frequency at different temperatures. The variation shows two different frequency regions in which changes are visible with the change in temperature. For the low frequency range, there was a monotonous decrease in the value of  $Z'$  with an increase in temperature. This behavior changed drastically in the high frequency region, which showed a complete merger of the  $Z'$  plot above a certain frequency ( $\sim 600$  kHz). At a particular frequency, the magnitude of  $Z'$  decreased with increasing temperature. This is a typical behavior of semiconductor materials. The plot of  $Z''$  with frequency at various temperatures, as shown in Figure 13, revealed that  $Z''$  values reached a maximum before decreasing with further increases of the applied frequency, indicating a single relaxation process in the studied device. The relaxation frequency ( $\omega_0$ ) corresponding to the  $Z''_{\max}$  shifted to higher frequency with increasing temperature. From the Arrhenius plot of  $\ln(\omega_0/T^2)$ , activation energy of the deep traps occurring at the CdS/CuO junction was subsequently calculated as 0.466 eV. The appearance of a discrete trapping level was consistent with the results observed in dc transport studies corresponding to SCLC conduction controlled by a single energy trap level.

In conclusion, copper oxide thin films were obtained by thermal oxidation of Cu thin films prepared by thermal evaporation in a vacuum at temperatures beyond 200°C. From the XRD patterns, the films oxidized at 500°C showed a pure CuO phase. The surface particle size and surface roughness increased with increasing thermal oxidation temperatures. A CdS/CuO heterojunction was successfully

fabricated by thermal evaporation of CdS thin films on CuO thin films obtained by oxidation at 500°C for 60 min. Three types of transport mechanisms controlled the forward current transport, namely: Ohmic conduction, recombination-tunneling, and space-charge limited current mechanisms, depending on the applied forward bias voltage. The real and imaginary parts of the complex impedance changed with the temperature and frequency. The experimental results suggested that the photovoltaic properties of the heterojunction diode should be studied further, as well as their potential use in photovoltaic devices with low thermal budget and low product cost.

### ACKNOWLEDGMENTS

The authors would like to thank Assoc. Prof. Dr. T. Wongcharoen and Asst. Prof. Dr. C. Poo-Rakkiat for their valuable input. This work was supported by King Mongkut's Institute of Technology Ladkrabang (grant number 2558A11802069/164817).

### REFERENCES

- Aksoy S., and Y. Cagar. 2012. Effect of ambient temperature on electrical properties of nanostructure n-ZnO/p-Si heterojunction diode. *Superlattices and Microstructures*. 51: 613-625. doi: 10.1016/j.spmi.2012.02.018.
- Aksoy, S., and Y. Cagar. 2014. Structural transformation of TiO<sub>2</sub> films with deposition temperature and electrical properties of nanostructure n-TiO<sub>2</sub>/p-Si heterojunction diode. *Journal of Alloys and Compounds*. 613: 330-337. doi: 10.1016/j.jallcom.2014.05.192.
- Barsoukov E., and J.R. Macdonald. 2005. *Impedance Spectroscopy: Theory, Experiment and Application*. 2<sup>nd</sup> Ed., John Wiley & Sons, New York.
- Cho, S. 2013. Optical and electrical properties of CuO thin films deposited at several growth temperatures by reactive rf magnetron sputtering. *Metals and Materials International*. 19: 1327-1331. doi: 10.1007/s12540-013-6030-y.
- Ooi, P.K., S.S. Ng, M.J. Abdullah, H. Abu Hassan, and Z. Hassan. 2013. Effect of oxygen percentage on the growth of copper oxide thin films by reactive radio frequency sputtering. *Materials Chemistry and Physics*. 140: 243-248. doi: 10.1016/j.matchemphys.2013.03.028.
- Rhoderick, E.H., and R.H. William. 1988. *Metal-Semiconductor Contacts*. 2<sup>nd</sup> Ed., Oxford University Press.
- Tyagi M., H. Toman, and V. Gupta. 2015. Trap assisted space charge conduction in p-NiO/n-ZnO heterojunction diode. *Material Research Bulletin*. 66:123-131. doi: 10.1016/j.materresbull. 2015.02.015.
- Valladares L.L.S., D.H. Salinas, D.A. Najarro, S.I. Khondake, T. Mitrelias, C.H.W. Barnes, J.A. Aguiar, and Y. Majima. 2012. Crystallization and electrical resistivity of Cu<sub>2</sub>O and CuO obtained by thermal oxidation of Cu thin films on SiO<sub>2</sub>/Si substrates. *Thin Solid Films*. 520: 6368-6371. doi: 10.1016/j.tsf.2012.06.043.

Zeyada H.M., M.M. El-Nahass, E.M. El-Menyawy, and A.S. El-Sawah. 2015. Electrical and photovoltaic characteristics of indium phthaloyanine chloride/p-Si solar cell. *Synthetic Metals*. 207: 46-53. doi: 10.1016 /j.synthmet.2015.06.008.